water

MDPI

Article

Runoff Simulation by SWAT Model Using High-Resolution Gridded Precipitation in the Upper Heihe River Basin, Northeastern Tibetan Plateau

Hongwei Ruan [1,2], Songbing Zou [3,4,*], Dawen Yang [5], Yuhan Wang [5], Zhenliang Yin [3], Zhixiang Lu [3], Fang Li [3] and Baorong Xu [4]

1 Key Laboratory of Water Cycle and Related Land Surface Processes, Institute of Geographic Sciences and Natural Resources Research, Chinese Academy of Sciences, Beijing 100101, China; ruanhw.17b@igsnrr.ac.cn
2 University of Chinese Academy of Sciences, Beijing 100049, China
3 Key Laboratory of Ecohydrology of Inland River Basin, Northwest Institute of Eco-Environment and Resources, Chinese Academy of Sciences, Lanzhou 730000, China; yinzhenliang@lzb.ac.cn (Z.Y.); lzhxiang@lzb.ac.cn (Z.L.); lifang162@mails.ucas.ac.cn (F.L.)
4 College of Earth Environmental Sciences, Lanzhou University, Lanzhou 730000, China; brxu@lzu.edu.cn
5 Department of Hydraulic Engineering, Tsinghua University, Beijing 100084, China; yangdw@tsinghua.edu.cn (D.Y.); wangyuh14@mails.tsinghua.edu.cn (Y.W.)
* Correspondence: zousongbing@lzb.ac.cn; Tel.: +86-093-1496-7144

Received: 25 September 2017; Accepted: 2 November 2017; Published: 7 November 2017

Abstract: The scarcity and uneven distribution of precipitation stations in the inland river basins of the Northeastern Tibetan Plateau restrict the application of the distributed hydrological model and spatial analysis of water balance component characteristics. This study used the upper Heihe River Basin as a case study, and daily gridded precipitation data with 3 km resolution based on the spatial interpolation of gauged stations and a regional climate model were used to construct a soil and water assessment tool (SWAT) model. The aim was to validate the precision of high-resolution gridded precipitation for hydrological simulation in data-scarce regions; a scale transformation method was proposed by building virtual stations and calculating the lapse rate to overcome the defects of the SWAT model using traditional precipitation station data. The gridded precipitation was upscaled from the grid to the sub-basin scale to accurately represent sub-basin precipitation input data. A satisfactory runoff simulation was achieved, and the spatial variability of water balance components was analysed. Results show that the precipitation lapse rate ranges from 40 mm/km to 235 mm/km and decreases from the southeastern to the northwestern areas. The SWAT model achieves monthly runoff simulation compared with gauged runoff from 2000 to 2014; the determination coefficients are higher than 0.71, the Nash–Sutcliffe efficiencies are higher than 0.76, and the percentage bias is controlled within ±15%. Meadow and sparse vegetation are the major water yield landscapes, and the elevation band from 3500 m to 4500 m is the major water yield area. Precipitation and evapotranspiration present a slightly increasing trend, whereas water yield and soil water content present a slightly decreasing trend. This finding indicates that the high-resolution gridded precipitation data fully depict its spatial heterogeneity, and scale transformation significantly promotes the application of the distributed hydrological model in inland river basins. The spatial variability of water balance components can be quantified to provide references for the integrated assessment and management of basin water resources in data-scarce regions.

Keywords: Heihe River Basin; SWAT model; gridded precipitation; water balance components; runoff simulation

1. Introduction

Changes in global climate and frequent harmful human activities have caused water shortage, which restricts the midstream social development and leads to downstream eco-environment degradation in inland river basins of Northwest China [1,2]. Runoff is generated mainly from cold mountainous regions, which significantly affects the midstream and downstream areas [3,4]. Hydrological models are widely used for the integrated assessment and management of basin water resources. Precipitation is an important input for accurate hydrological simulation, and its numerical accuracy and detailed spatial distribution are necessary [5,6]. However, precipitation gauge stations are scarce and unevenly distributed in the cold mountainous regions of Northwest China because of economy, terrain, transport, and technology limitations [7]. Thus, these gauge stations barely represent the spatial heterogeneity of regional precipitation, therefore leading to high uncertainty in hydrological simulation and analysis. Alternatively, this data-scarce situation can be addressed by using high-resolution gridded precipitation.

Gridded precipitation based on gauge stations has been widely investigated and used to establish hydrological models. Version 6 of the global precipitation product developed by the Global Precipitation Climatology Centre has monthly resolutions of 0.5° from 1901 to 2010 [8]. Li et al. [9] and Huang et al. [10] used the spline interpolation and trend surface methods to determine gridded precipitation in China. Yang et al. [11] evaluated different gridded precipitations to establish a hydrological model of the Three Gorges Reservoir. Fuka et al. [12] used National Centrer for Environmental Prediction Climate Forecast System Reanalysis data to construct a hydrological model for validating the accuracy of gridded precipitation. Previous studies also used sparse meteorological stations to construct gridded precipitation in China; these stations poorly represent the amount and spatial distribution of precipitation [13]. By contrast, hydrological stations can provide gauged precipitation to complete precipitation data; the regional climate model (RCM) can also supply information on spatial distribution to correct gridded precipitation [14]. Gridded precipitation data with daily resolutions of 3 km have been developed for the Heihe River Basin (HRB) through spatial interpolation of meteorological station, hydrological station, and Regional Integrated Environmental Model System (RIEMS) RCM simulation. This high-resolution gridded precipitation can fully depict spatial heterogeneity, which is preferred for hydrological simulation and analysis [15,16]. This gridded precipitation exhibits certain credibility, but few researchers use it to analyse the climate and hydrology characteristics in the upper HRB.

The hydrological model has been increasingly used to analyse the hydrological process in the HRB; water shortage problems are typical of the inland river basins of Northwest China. Soil and water assessment tool (SWAT) is a physical, semi-distributed hydrological model that has a few advantages in predicting climate change effects on water-related and hydrological processes over a continuous time [17]. The performance of this model relies on precipitation input parameters, namely accuracy and spatial distribution [18]. So, many researchers have selected grid precipitation to drive hydrological models. Evans et al. [19] used four RCMs coupled with a CMD-IHACRES hydrological model to compare the different results. Lakhatkia et al. [20] coupled MM5 with a THM hydrological model to study water resources and hydrological process response to climate change scenarios. Zou et al. [21] used RIEMS simulation as driving data for a SWAT model to improve monthly runoff simulation in the upper HRB. Most studies that directly input grid data into the hydrological model cannot maximise the precision of high-resolution data because most grids are ignored [22]. The SWAT model employs precipitation data from only one station closest to the centroid of each sub-basin, which can be corrected by elevation band and lapse rate; thus, the current method of representing precipitation in the SWAT model is simple. Accordingly, sub-basin precipitation input data are inaccurately represented [23]. The SWAT model applied to the upper HRB focuses on model modification and hydrological process responses to climate and land use change; thus far, few studies have optimised precipitation input parameters using gridded data [24–28]. Therefore, a reasonable scale transformation from the grid to the sub-basin must be developed to maximise the precision of high-resolution gridded data. By this method one can overcome the model structure defects and improve model input parameters. The suitability of the hydrological model in data-scarce regions can be improved by scale transformation of high-resolution

gridded precipitation. Moreover, the water balance components should be accurately described to provide a reference scheme for similar hydrological models when using high-resolution gridded climate data in data scarce regions. The spatial variability of water balance components can be quantified to assess and manage water resources in the upper HRB [29]. Water balance components cannot be directly measured but can be calculated by the SWAT model. The SWAT model can simulate water balance components with high accuracy and detailed spatial distribution depending on the inputs of high-resolution gridded precipitation. Currently, water balance components are estimated at different scales, namely, global, regional, watershed, and ecosystem levels [30–33]. Thus, the spatial distribution, change trends, and internal relationship of water balance components across different scales can further strengthen the understanding of the hydrological processes.

This study regarded the upper HRB as a case study, and gridded precipitation with 3 km resolutions was used to construct a SWAT model. A scale transformation method was proposed to overcome the structure defects of the SWAT. The gridded precipitation was upscaled from the grid to the sub-basin scale to accurately represent sub-basin precipitation input data. The spatial distribution, change trends, and internal relationship of water balance components across different scales were analysed based on the model simulation. The main content includes: (1) assessing the quality of gridded precipitation data in the upper HRB; (2) conducting scale transformation by building virtual precipitation stations to transfer gridded data into a sub-basin average and calculating precipitation lapses rates on the sub-basin scale, thereby optimising the input parameters of precipitation; (3) assessing the performance of the SWAT model by comparing the monthly runoff simulation with observed data; and (4) analysing the spatial variability and change trend of water balance components on the sub-basin, landscape, and elevation band scales on the basis of the simulation results.

2. Study Area and Data Availability

2.1. Study Area

The HRB is the second largest inland river basin in Northwest China, originates from the Qilian Mountains in the Northeastern Tibetan Plateau and flows through the middle of the Hexi Corridor, which was an important district of the ancient Silk Road [34]. The upper HRB generates approximately 70% of the river flows of the entire basin, which supports the social development of the midstream and maintains the eco-environment balance of the downstream [1]. This study focused on the upper HRB with a drainage area of approximately 10,009 km^2 and covered by mountainous terrain (Figure 1). The elevation of the study area ranges from 1667 m to 5008 m, with a mean elevation of 3737 m. The basin outlet is monitored by the Yingluoxia hydrological station. Hydrological stations in Qilian and Zhamashike are situated in the east and west tributaries of the upper HRB, respectively [35]. The flow of the two tributaries joins the mainstream at the Huangzangsi and enters the basin outlet. The basin comprises three subregions, namely, the east tributary, west tributary, and mainstream. The study area, which is a typical inland region with large spatiotemporal variability, experiences a dry and cold climate in winter and a moist and hot climate in summer. The mean annual precipitation varies from 200 mm to 700 mm, decreases from the southeast to the northwest, and increases along with elevation; approximately 60% of the precipitation occurs in the summer. The mean annual temperature in this region ranges from −5 °C to 4 °C [27,36]. The glacier area is approximately 34.8 km^2, which accounts for 0.35% of the basin area and contributes 3% of the runoff [37]. The landscape follows a distinct vertical zonation and comprises the desert, steppe, shrub, coniferous forest, meadow, sparse vegetation, snow, and glaciers, which vary from low to high elevations. The major soil types in the basin are felty, chestnut, and alpine frost soils [38].

2.2. Data Availability

The data used in this study were categorised into data on geospatial information and climate forcing for the SWAT model setup and data on gridded precipitation assessment and data on SWAT model validation. The meteorological data were daily temperature, sunshine hour, wind speed, and relative

humidity, which served as climate forcing data. These data were downloaded from the National Meteorological Stations of China Meteorological Administration (CMA). Gridded precipitation data with daily resolutions of 3 km were used as precipitation forcing data downloaded from the Heihe Plan Science Data Centre (HPSD), which was developed by Wang et al. [15]. A digital elevation model with 90 m resolution was downloaded from the SRTM database [39]. The soil map of the upper HRB was derived from the Second National Soil Survey of China. The vegetation map, with a measuring scale of 1:100,000, was obtained from the HPSD; the vegetation pattern boundary was adjusted relative to that of the previous version (Figure 2). The gauged precipitation data, including two experimental stations, four meteorological stations, and 13 hydrological stations, were obtained from CMA and HPSD and used to evaluate gridded precipitation (Figure 1). The daily gauged runoff data were obtained from the Hydrology and Water Resources Bureau of Gansu Province and used to validate the SWAT model.

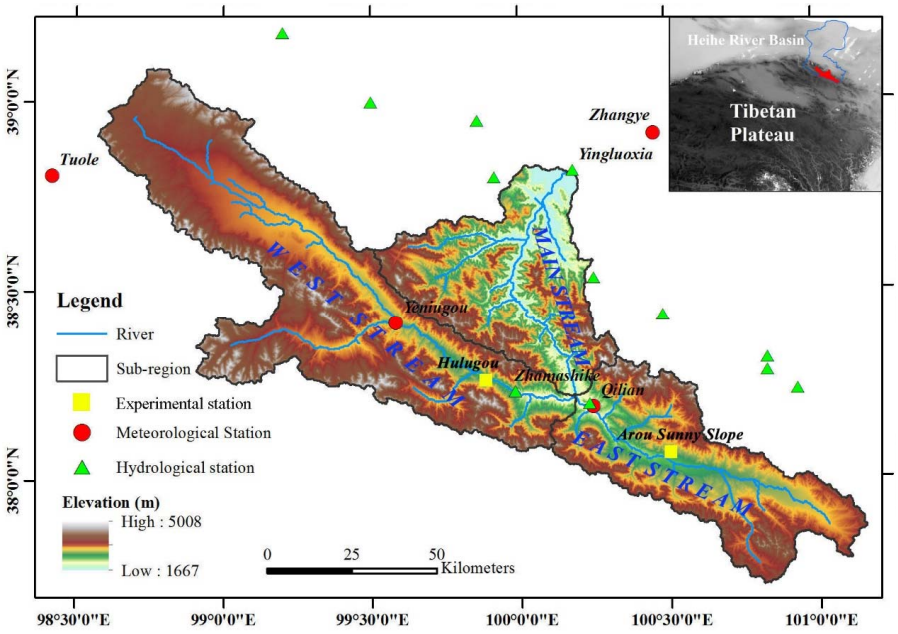

Figure 1. Upper Heihe River Basin.

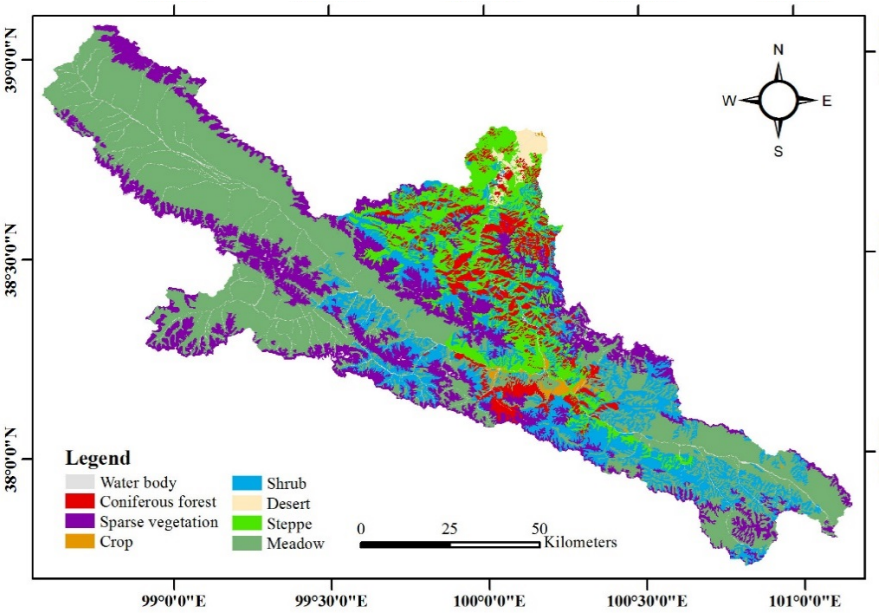

Figure 2. Vegetation map of the upper Heihe River Basin.

3. Methods

3.1. SWAT Model

The SWAT model is a physical, semi-distributed hydrological model that can operate under different climate conditions and land use change scenarios. The model is widely used to simulate long-term yields in large watersheds for the assessment and management of water resources [17]. The runoff transport process considered in the SWAT model includes watershed land areas that transport water to the channels and through the stream network to the watershed outlet [40]. The basin is divided into hydrologic response units (HRUs) that integrate unique land use, soil type, and slope, which are the basic elements of hydrological calculation. The HRUs of water balance components, such as precipitation, evapotranspiration, water yield, surface flow, lateral flow, and groundwater flow, were calculated [41]. The hydrological processes simulated by the SWAT model are based on the following water balance equation:

$$SWt,i = SW_0,i + \sum_{i=1}^{t} (Qday,i - Qsurf,i - Ea,i - Wseep,i - Qgw,i), \quad (1)$$

where $SW_{t,i}$ is the final soil water content (mm H_2O), $SW_{0,i}$ is the initial soil water content on day i (mm H_2O), t is the time (days), $Q_{day,i}$ is the amount of precipitation on day i (mm H_2O), $Q_{surf,i}$ is the surface runoff amount on day i (mm H_2O), $E_{a,i}$ is the amount of evapotranspiration on day i (mm H_2O), $W_{seep,i}$ is the amount of water that enters the vadose zone from the soil profile on day i (mm H_2O), and $Q_{gw,i}$ is the return flow amount on day i (mm H_2O).

3.2. Gridded Precipitation

The gridded precipitation data were spatially interpolated using the method developed by Shen and Xiong [13]. Firstly, a gridded analysis of daily precipitation climatology was built on the basis of the inverse distance weighting interpolation method and mean daily gauged precipitation data from 1960 to 2014. The gauged precipitation, including meteorological stations and hydrological stations of the entire HRB, was smoothed by Fourier transformation to remove high-frequency noise precipitation caused by insufficient sampling, real extreme events, and random measurement errors. Secondly, the RIEMS RCM provided the spatial distribution of the precipitation lapse rate [14]. RCM simulation was used to correct the precipitation lapse rate of daily precipitation climatology. Thirdly, Optimal Interpolation (OI) was employed to create the gridded ratio field, which is the ratio of the daily gauged precipitation to daily precipitation climatology [42]. Finally, the gridded precipitation was calculated by multiplying the daily gridded precipitation climatology by the daily gridded precipitation ratio. Gridded precipitation data with daily resolutions of 3 km for a time series were generated over the HRB [2,4,15,16].

3.3. Virtual Precipitation Station

The precipitation data are inputted to the SWAT model in the form of station data, and then the precipitation station data are discretised to sub-basin scale and can be corrected by the elevation band and lapse rate [17]. Thus, the grids of gridded precipitation data are treated as a virtual precipitation station, and a virtual station is a common method that grids data input to the SWAT model [21,22,43,44]. However, the SWAT model only uses station data closest to the centroid of each sub-basin. High-resolution gridded data are converted into abundant virtual stations, bu the quantity of the sub-basin cannot be fully matched with the resolution of gridded precipitation. The abundant virtual stations are directly inputted to the SWAT model, which leads to the inaccurate representation of the sub-basin precipitation input data because most virtual stations are ignored [45]. Hence, the current method of representing precipitation in the SWAT model cannot fully reflect the

high-resolution superiority of gridded data. Therefore, a reasonable method of building virtual stations must be developed.

In this study, virtual precipitation stations were built for each sub-basin that adopts the mean precipitation of the grid within each sub-basin; all grid data could be utilised to build virtual stations on a sub-basin scale. Precipitation was transferred from grid into a sub-basin average by building virtual station and then into SWAT. Thus, the precision of gridded data in horizontal distribution can be maximised, and the representation of sub-basin precipitation input data can be improved. The virtual precipitation stations were built through the following steps: (1) the spatial distribution of the sub-basin was pre-divided, and a grid-sized buffer of the sub-basin boundary was set; (2) the grid precipitation data were converted into point data with the grid centre as the spatial position; (3) the mean precipitation of all points within the boundary of each sub-basin was calculated and used as values for the virtual precipitation station; and (4) the longitude and latitude of the sub-basin centroid used directly used as the spatial position of the virtual precipitation station to ensure that each sub-basin reads only one specified station. The virtual station elevation was calculated by the mean elevation of all points within the boundary of the sub-basin.

3.4. Precipitation Lapse Rate

Precipitation significantly varies with elevation because of the relatively complicated terrain in the mountainous region. The SWAT model allows the division of the sub-basin into the elevation bands and sets the precipitation lapse rate to correct the vertical precipitation variability to represent the precipitation variability caused by elevation changes [46]. Previous studies usually regarded the precipitation lapse rate as a calibrated parameter, thereby leading to low spatial heterogeneity and high precipitation uncertainty. High-resolution gridded precipitation with detailed and accurate information of vertical distribution requires the calculation of precipitation lapse rate on the sub-basin scale. In this study, the lapse rate for each sub-basin was calculated; the lapse rate served as input parameters for the SWAT model. The precision of the gridded precipitation in vertical distribution can be maximised using this method, and the precipitation input parameters for the SWAT model can be optimised.

Several studies used linear regression models to analyse the precipitation variability with elevation in the upper HRB [47,48]. Linear regression functions were used to calculate the precipitation lapse rate on the sub-basin and mean annual scale. The linear regression function is shown in Equations (2) and (3):

If:

$$P = plr \times H - a \tag{2}$$

then:

$$plr = (P + a)/H, \tag{3}$$

where plr is the precipitation lapse rate (mm/km), P is the precipitation at different grids, a is the precipitation at the base location of sub-basin, and H is the elevation at different grids.

4. Results

4.1. Assessing Gridded Precipitation

The upper HRB is located in the inland and alpine cold mountainous region, where precipitation is influenced mainly by westerlies and the Pacific monsoon. Precipitation in the upper HRB also exhibits large spatiotemporal variability because of convection in mountainous terrain [49,50]. Given the complicated mountainous terrain, the quality of gridded precipitation in the upper HRB was assessed. Gridded precipitation was assessed at time series accuracy and spatial description capability. Gauged precipitation of the Hulugou and Arou sunny slope experimental stations was selected to compare with the gridded data, which have not been used in the interpolation. The two stations are located in the east and west tributaries of the basin, which ensures high representativeness.

Precipitation gauged by four meteorological stations and 13 hydrological stations was also used to evaluate the vertical distribution of precipitation.

4.1.1. Assessing Gridded Precipitation

Time series accuracy was evaluated by comparing gauged precipitation with the nearest pixel of gridded precipitation in a time series to assess the performance of the gridded data during the period from 2011 to 2014. Figures 3 and 4 show the daily and monthly comparison results in the Hulugou and Arou sunny slope stations, respectively. In the scatter diagram, no precipitation days are ruled out. The points are symmetrically distributed on both sides of the 1:1 lines. The point distribution is scattered, and the correlation is high. The comparison of the monthly results indicates that the monthly gridded precipitation is close to the gauged precipitation, and their change trends are consistent. However, the Arou sunny slope station lacks snowfall observation, and thus, the bias is large before April and after September [15].

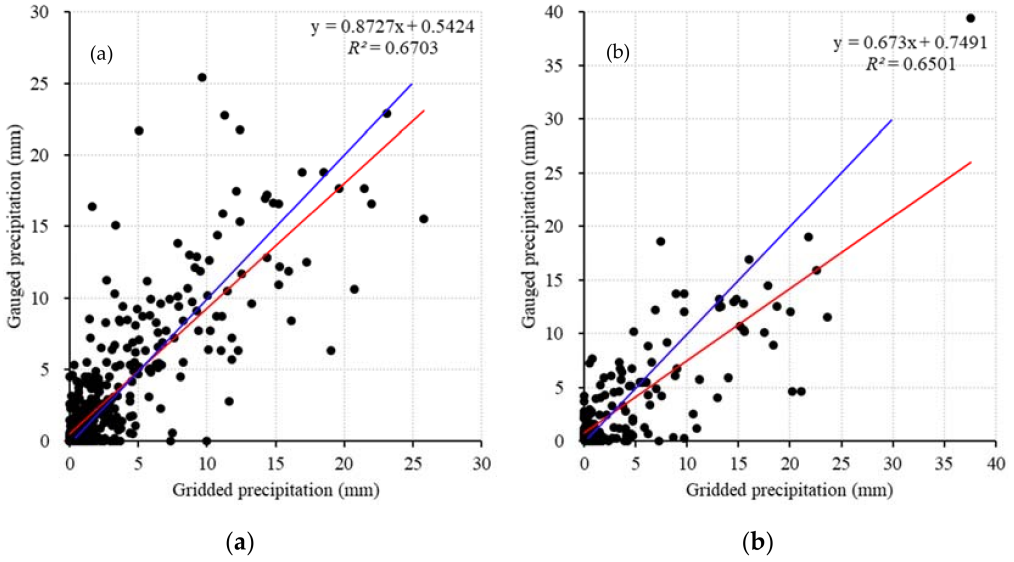

(**a**) (**b**)

Figure 3. Scatter diagram of daily gauge precipitation and daily gridded precipitation in Hulugou (**a**) and Arou sunny slope (**b**) (red line, trend line; blue line, 1:1 line).

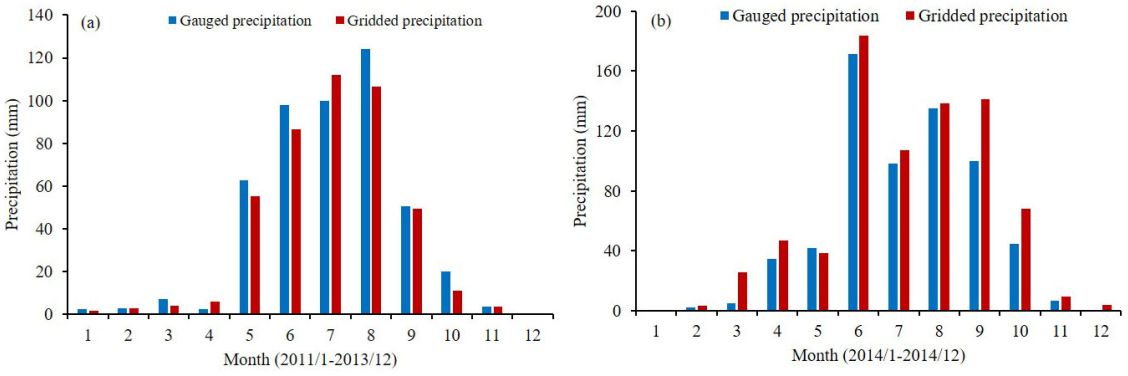

Figure 4. Comparison of monthly gauge precipitation and gridded precipitation in Hulugou (**a**) and Arou sunny slope (**b**).

In this study, determination coefficients (R^2), root-mean-square error (RMSE), and percent bias (PBIAS) were used to assess the quality of the gridded precipitation data [51–53]. Table 1 shows the criteria used to evaluate gridded data in Hulugou and Arou sunny slope. At the yearly scale, the mean annual gridded precipitation is slightly lower than Hulugou and obviously larger than

Arou sunny slope. The R^2 values of Hulugou and Arou sunny slope at the daily scale reached 0.67 and 0.65, respectively; the R^2 values at the monthly scale reached 0.95 and 0.96, respectively, indicating a strong correlation. The daily and monthly scales of PBIAS are controlled within ±20%. The RMSE values are approximately 3 mm at the daily scale and 17 mm at the monthly scale; the error is low. The Arou sunny slope lacks snowfall observation and, thus, the bias is large. In summary, the gridded precipitation data exhibit satisfactory performance in terms of time series accuracy.

Table 1. Simulated evaluation of temperature, specific humidity, and wind speed.

Station	Yearly Scale		Daily Scale			Monthly Scale		
	Gauge Data (mm)	Gridded Data (mm)	R^2	RMSE (mm)	PBIAS (%)	R^2	RMSE (mm)	PBIAS (%)
Hulugou	474.3	439.6	0.67	1.78	7.31	0.95	10.78	7.31
Arou sunny slope	639.4	766.4	0.65	2.57	−19.87	0.96	16.12	−19.87

4.1.2. Spatial Description Capability

The precision of high-resolution gridded precipitation is attributed to its spatial description capability; thus, the spatial distribution of precipitation must be assessed. Figure 5 shows the mean annual precipitation distribution of the gridded data during the period from 2000 to 2014. The mean annual gridded precipitation values in the entire basin, the east tributary, the west tributary, and the mainstream are 513, 589, 505, and 422 mm, respectively. In the basin, precipitation decreases from the southeast to the northwest, and precipitation from the south face is higher than that from the north face. The high precipitation zone occurs in the northern east tributary, and the low precipitation zone occurs in the basin outlet. The elevation band of the high precipitation occurred from 4300 m to 4800 m. A previous study reported that the location of the high precipitation band is related to the degree of dryness and wetness. In the middle of the north face of the Qilian Mountains, the maximum wetness degree elevation is 4600 m; the high precipitation band ranges from 4500 m to 4700 m [50,54,55]. These conclusions are consistent with those for the gridded precipitation distribution. However, gridded precipitation is overestimated in high-altitude areas compared with previous studies [27,56].

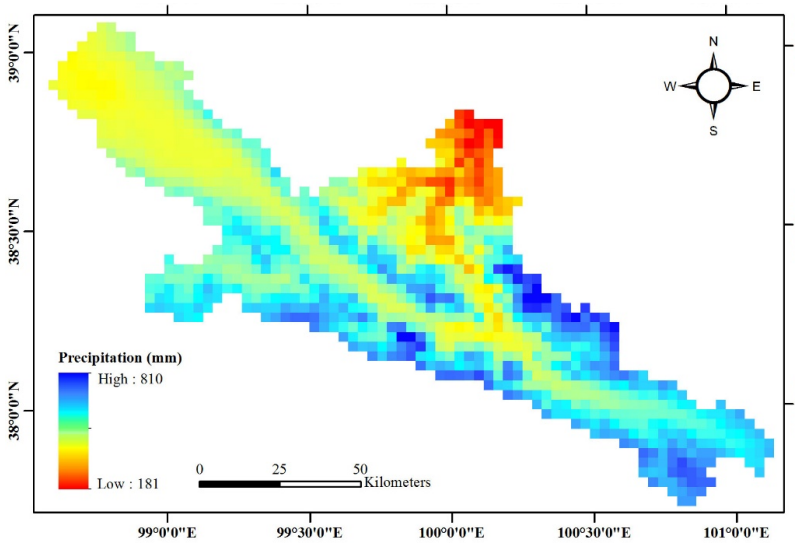

Figure 5. Distribution of the average annual gridded precipitation.

The spatial precipitation distribution is strongly correlated with elevation (Figure 5). Apparently, the mean annual gridded precipitation is high in the high-altitude area and low in the

river valley area. Figure 6 shows the scatter diagram of the mean annual gridded precipitation and its elevation. For the east tributary and mainstream, the R^2 values reach 0.89 and 0.74, respectively, indicating apparent strong correlations. The precipitation lapse rate of the east tributary and the mainstream is 165 mm/km, which is close to the precipitation lapse rate from the observation data (171 mm/km). Notably, the R^2 value of the west tributary is the lowest (0.16), and its precipitation lapse rate is 84 mm/km. The R^2 value of the entire basin is 0.37, and its precipitation lapse rate is 120 mm/km. The east tributary and the mainstream are stronger than the west tributary in terms of precipitation lapse rate. The spatial precipitation lapse rate distribution is consistent with the findings of Chen and Liu [47,48]. The precipitation lapse rate of the west tributary is lower than that of the east tributary, mainstream and entire basin. Most of the gauged stations are located in the valley and shallow mountainous areas, with elevations all lower than 3500 m. Most stations are near the east tributary and mainstream areas. Thus, the gauge stations lack representativeness for the west tributary. Nevertheless, the spatial precipitation lapse rate distribution has a certain reference value. In summary, gridded precipitation and elevation exhibit an obvious linear regression relationship; that is, precipitation increases with elevation. In addition, gridded data can be used to describe the horizontal and vertical precipitation distribution in the study area.

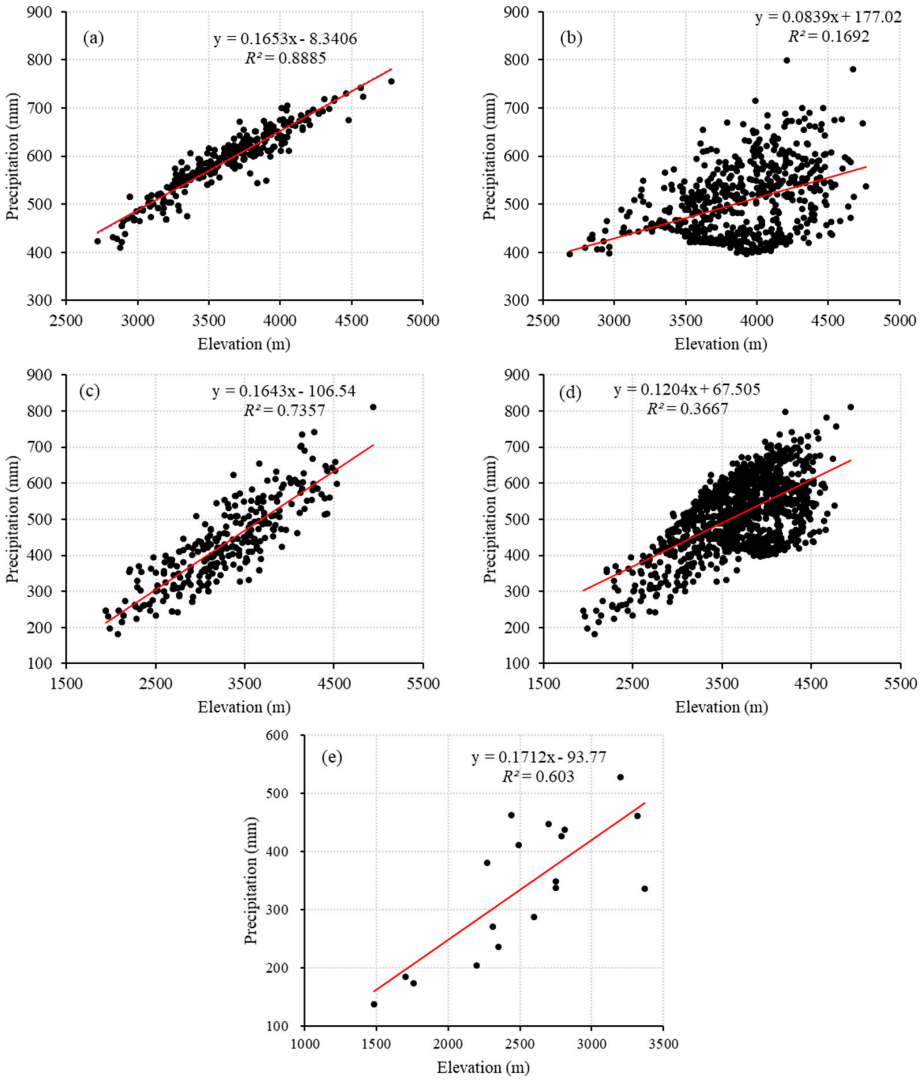

Figure 6. Scatter diagram of the gridded precipitation and its elevation in the east tributary (**a**), west tributary (**b**), mainstream (**c**), entire basin (**d**), and observations (**e**).

4.2. Distribution of Virtual Stations

The spatial discretisation scheme of the SWAT model for precipitation is classified as a lumped type and uses data from the grid closest to the centroid of each sub-basin. The distribution and numbers of the sub-basin can be used to determine where and how many grids can be introduced into the SWAT model. The total number of grid data within the upper HRB reaches 1113 if direct input gridded precipitation rendering most grids is ignored. Scale transformation by building virtual precipitation stations is important for grid upscale to sub-basin scale. Thus, the drainage area threshold of the sub-basin division is critical for scale transformation, which determines the distribution and number of the sub-basin. The setting of drainage area threshold considers regional climate and terrain features, which influence the hydrological processes. The SWAT model can generate a large number of sub-basins and independent geographical area. In accordance with studies on the optimal drainage area threshold for the upper HRB, the drainage area threshold was set at 50 km^2 [35]. The SWAT model generates 97 sub-basins. The centroid of each sub-basin was considered a virtual precipitation station that adopts the mean precipitation of the grid within each sub-basin. From the distribution and number of sub-basins, 97 virtual precipitation stations of time-series were built to transfer gridded data into a sub-basin average (Figure 7). By this method, the SWAT model can reasonably discretise sub-basin precipitation input data. Scale transformation can effectively maximise the precision of the gridded precipitation in horizontal distribution and optimise the precipitation inputs for the SWAT model.

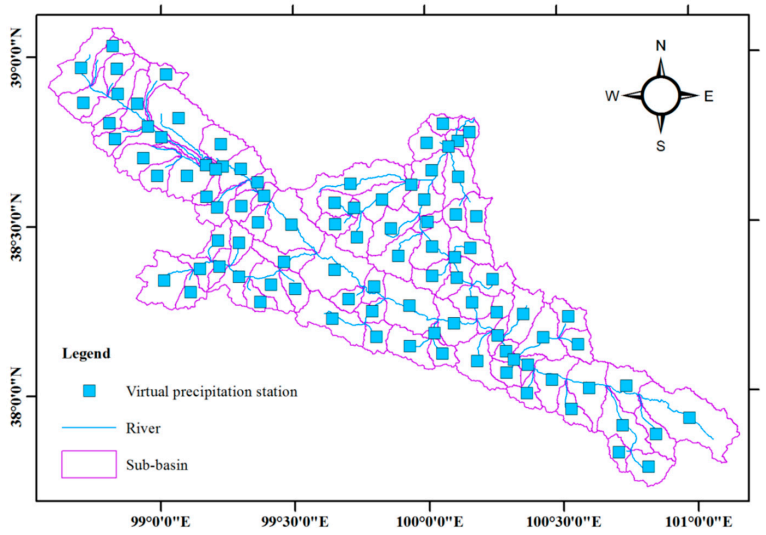

Figure 7. Distribution of the virtual precipitation station.

4.3. Distribution of Precipitation Lapse Rate

Precipitation and elevation exhibit a linear regression relationship in the upper HRB; thus, linear regression functions are widely used to compute precipitation lapse rate [48]. The linear regression functions of the mean annual gridded precipitation and elevation were established to calculate the precipitation lapse rate at the sub-basin scale. Finally, the precipitation lapse rates of 97 sub-basins were obtained (Figure 8). A total of 500 m interval was used to divide the elevation bands for the sub-basin. The precipitation lapse rate and elevation bands were combined to correct the vertical distribution of precipitation, thereby maximising the precision of the high-resolution gridded precipitation.

Figure 8 shows the decreasing trend of the precipitation lapse rate from the southeastern to the northwestern areas; the change trends and spatial distribution are consistent with those of precipitation. The precipitation lapse rate ranges from 40 to 235 mm/km and decreases from southwest to northwest. The mean precipitation lapse rates are 120 and 165 mm/km in the entire basin and in the east tributary and mainstream, respectively. The precipitation lapse rate of the west tributary is 84 mm/km. In summary, the

distribution of the precipitation lapse rate is consistent with the previously reported precipitation lapse rate in the upper HRB [47,49]. Thus, a linear regression function of precipitation and elevation is appropriate for calculating the precipitation lapse rates.

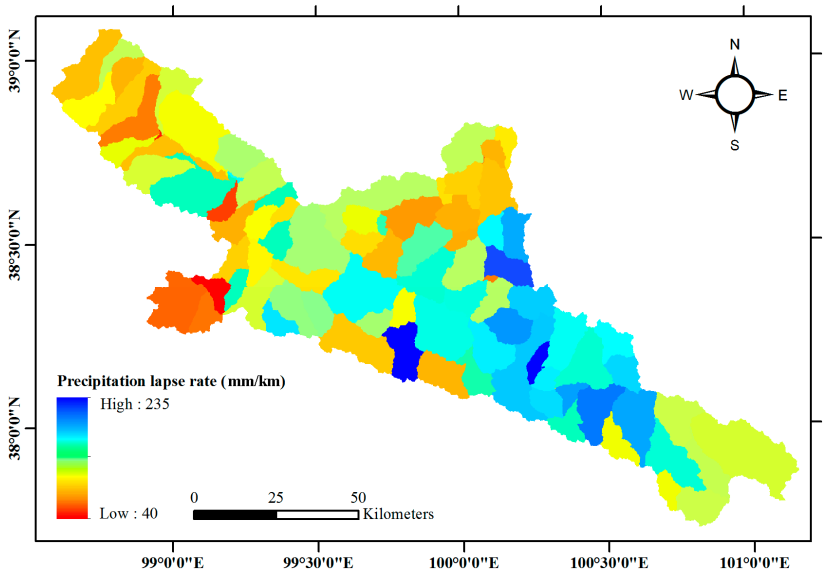

Figure 8. Distribution of the sub-basin precipitation lapse rate.

4.4. Model Calibration and Performance

The applications of the SWAT model on the large-scale and long-term series simulations are concentrated mainly on the monthly scale, and most hydrological models have simulated monthly runoff in the upper HRB [4,57–59]. This study simulated monthly runoff and evaluated on the basis of monthly scale, and the hydrological process was analysed from the monthly simulation results. The SWAT simulation results can be compared with similar hydrological models in this study area. The SWAT model was used to simulate the monthly runoff from January 2000 to December 2014. The model was calibrated for the period from January 2003 to December 2008 and validated for the period from January 2009 to December 2014; the period from January 2000 to December 2002 was regarded as the warm-up period. The hydrologic calibration followed multi-temporal, multi-variable, multi-site principles and used the observed data, hydrological characteristics, and expert knowledge of the basin to improve the accuracy of the runoff simulation [60]. Parameter sensitivity was analysed by SWAT-CUP in the upper HRB. The 10 most sensitive parameters in the three sub-regions were manually calibrated and validated on the basis of expert knowledge. Table 2 shows the most sensitive parameters and their fitted values.

The SWAT model used the observed and simulated monthly runoff statistics at three hydrological stations (Qilian, Zhamashike, and Yingluoxia). Three goodness-of-fit measures, namely, R^2, Percentage bias (PBIAS) and Nash–Sutcliffe efficiencies (NS), were used [51–53,61]. The runoff simulated by the SWAT model was compared with the observed runoff at the three hydrological stations. The seasonal dynamics of the simulated runoff in the hydrographs are consistent with the observed runoff, except for Qilian and Zhamashike, which exhibit poor performance at the peak value in some years (Figure 9). Statistical analyses of the calibration and validation periods show that the R^2 values range from 0.76 to 0.93, indicating that the simulation exhibits a strong correlation with the observation findings. The NS values range from 0.71 to 0.92, exhibiting the high credibility of the simulation. The PBIAS values range from −14.02% to 11.51%, indicating that the model overestimates the runoff in the calibration period and underestimates the runoff in the validation. However, the PBIAS values are still within a reasonable range. In general, the model performance in the validation period is better than the model performance in the calibration period.

Table 2. Most sensitive parameters.

Parameter	Description	Range	Value	Sensitivity
Ch_K2	Effective hydraulic conductivity in main channel alluvium (mm/h)	0–500	8–15	1
Cn2	Initial SCS runoff curve number for moisture condition II	35–98	43–95	2
Plaps	Precipitation lapse rate (mm/km)	−1000–1000	40–235	3
Esco	Soil evaporation compensation factor	0–1	0.83–0.90	4
Alpha_Bf	Base flow alpha factor (days)	0–1	0.06–0.072	5
Smfmn	Melt factor on 21 December (mm H_2O/°C day)	0–20	1	6
Sol_Awc	Available water capacity of the soil layer (mm H_2O/mm soil)	0–1	0.1–0.22	7
Tlaps	Temperature lapse rate (°C/km)	−10–10	−5	8
Gw_Delay	Groundwater delay time (days)	0–500	31	9
Smfmx	Melt factor on 21 June (mm H_2O/°C day)	0–20	2.5	10

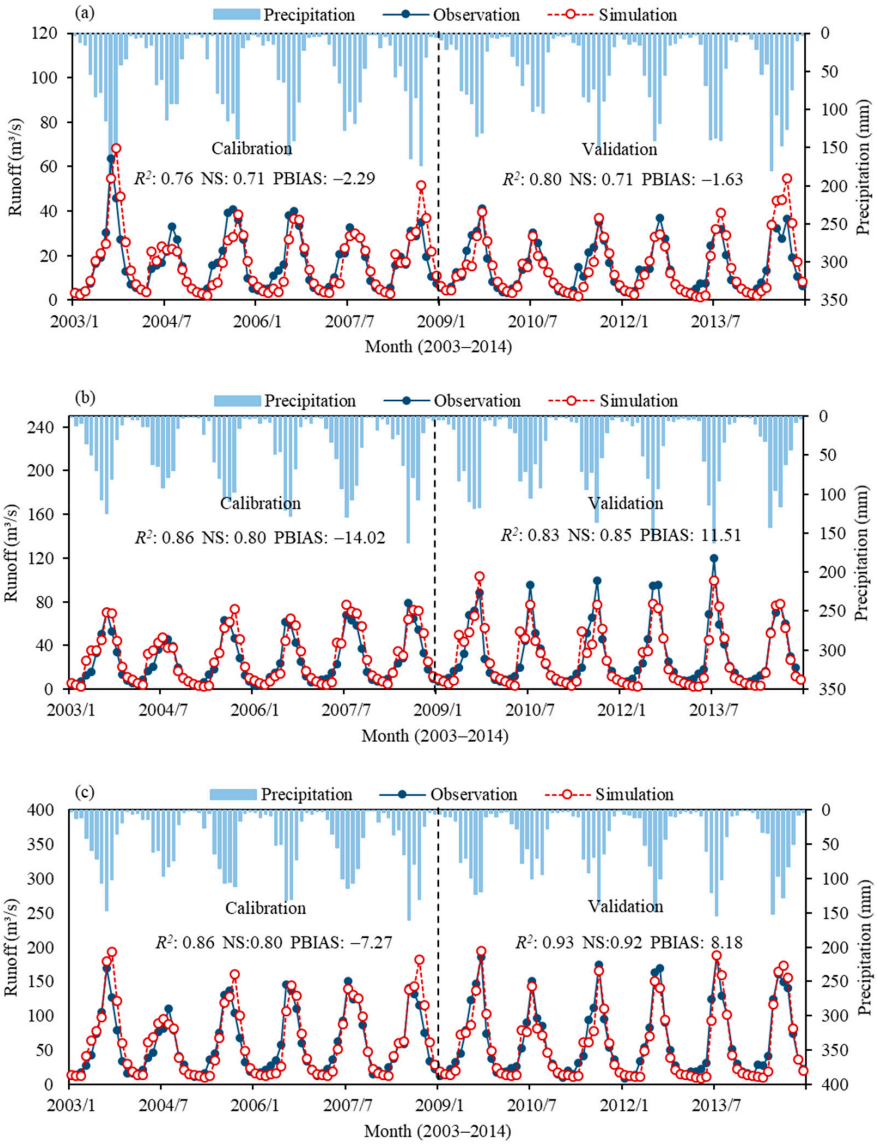

Figure 9. Monthly observation and simulated runoff of Qilian (**a**), Zhamashike (**b**), and Yingluoxia (**c**).

The daily runoff simulation and previous studies on regional meteorological and hydrological characteristics can also provide references to validate the SWAT model application better. Considering the daily time step with a high uncertainty, the daily runoff simulated by the SWAT model was compared with the observed runoff at the Yingluoxia station in 2007 and 2013 (Figure 10). The two years are typical normal and high flow year and exhibit high representativeness. The daily dynamics of the simulated runoff in the hydrographs are consistent with the observed runoff. The R^2 values are higher than 0.60, the NS values are higher than 0.70 and the PBIAS values are controlled within ±10%, indicating that the model exhibits satisfactory performance on the daily scale. The base flow coefficient based on the model simulation is 0.46, which is close to the result in the base flow separation (0.44) [62]. The hydrographs show that the model performs well during the snowmelt period (April to May). Furthermore, the hydrographs indicate that the snowmelt runoff simulation is reasonable. The actual evapotranspiration is 318 mm, which is close to the remote sensing data (306 mm) [63]. The potential evapotranspiration estimated by the SWAT model is 575.3 mm, which is higher than the potential evapotranspiration estimated by HBV runoff model simulation (500.4 mm) [37].

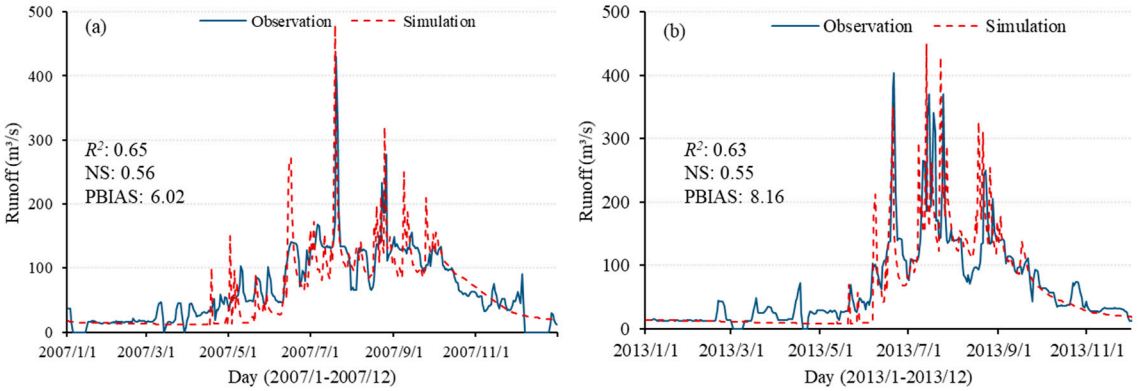

Figure 10. Daily observation and simulated runoff of Yingluoxia in 2007 (**a**) and 2013 (**b**).

In summary, the simulation results exhibit good and very good performance that satisfies the accuracy and reliability requirements of the SWAT model, respectively [64]. The simulation with the SWAT model used high-resolution gridded precipitation and comprised building virtual stations and calculating lapse rates to optimise the precipitation input parameters and improve the hydrological simulation. After using high-resolution gridded precipitation, the model can simulate accurate and detailed spatial distribution of water balance components, thereby improving the understanding of the regional hydrological processes.

4.5. Water Balance Component Characteristics

Water balance components, including precipitation (PREC), evapotranspiration (ET), water yield (WYLD) and soil water content (SW), which is a mean value at annual scale during the period of 2003–2014, were considered in this study. Table 3 shows the mean annual values of the water balance components from 2003 to 2014 in different regions. The precipitation, evapotranspiration and water yield for the entire basin are 525.5, 318.1 and 194.4 mm·year^{-1}, respectively, indicating that the water balance components are relatively balanced. The mean annual precipitation is close to the original gridded precipitation (513 mm·year^{-1}), indicating that the scale transformation and precipitation lapse rate calculation are reasonable. The evapotranspiration is similar to the remote sensing data (306 mm·year^{-1}) [63]. The differences of water balance components in different regions were determined by precipitation. The runoff coefficients in different regions are similar, and the coefficient of the entire basin is 0.37.

Table 3. Water balance components for different regions.

Region	Area (km^2)	PREC (mm)	ET (mm)	WYLD (mm)	SW (mm)	Runoff Coefficient	Runoff Contribution (%)
East Tributary	2504	609.8	364.4	229.9	63.5	0.37	29
West Tributary	5032	522.8	310.3	199.5	58.5	0.38	52
Main Stream	2482	446.2	287.4	148.3	27.7	0.33	19
Entire Basin	10018	525.5	318.1	194.4	52.1	0.37	100

4.5.1. Spatial Variability of Water Balance Components at the Landscape Scale

Figure 11 shows the percentage, runoff contribution and runoff coefficient of water balance components on the landscape scale. The meadow is the dominant vegetation type, which accounts for 43.8% of the basin area and contributes 44.8% of the runoff. The runoff coefficient of the meadow is 0.37, which is equal to that of the entire basin. The area of sparse vegetation accounts for 19.6% of the basin area and contributes 23.6% of the runoff. The runoff coefficient of sparse vegetation is the highest (0.42) at all of the landscapes. The sparse vegetation is generally distributed at high-altitude areas with low temperatures, high precipitation and alpine cold desert. Thus, the evapotranspiration and soil water content in this area are low, and the runoff coefficient is high. The shrub accounts for 16.8% of the basin area and contributes to 17.2% of the runoff. The meadow, sparse vegetation and shrub account for 79.4% of the basin area and contribute 85.6% of the runoff, and they are the main water yield landscapes. Steppe and coniferous forests account for 17.2% of the basin area and contribute 12.2% of the runoff. However, their runoff coefficients are low because of the interception of the canopy and roots. Thus far, whether the forests in the alpine cold mountain region generate runoff remains unclear. The forest in the study area includes coniferous forest and shrub, which contribute 4.5% and 17.2% of the total runoff, respectively. These results are similar to the findings of the small catchment experiment and hydrological simulation in the upper HRB [29,65]. The water body includes river, snow and glacier, and the runoff coefficient is high. The desert and crop areas are lower and contribute only 0.6% of the total runoff.

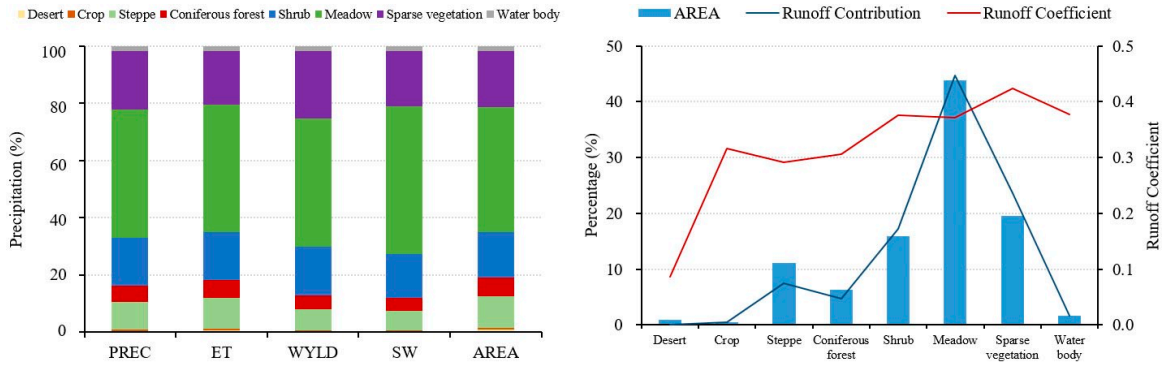

Figure 11. Spatial variability of water balance components at the landscape scale and their runoff coefficients.

4.5.2. Spatial Variability of Water Balance Components at the Elevation Band Scale

Elevation significantly affects the hydrological processes in alpine cold mountainous regions. The landscape follows a distinct vertical elevation band, but the elevation band presents obvious boundaries that may be composed of different landscape. The spatial variability of water balance components on elevation band scale differs and should be analysed.

According to the vertical distribution of vegetation, the basin was divided into five elevation bands, namely 1667–2800, 2800–3500, 3500–4000, 4000–4500, and 4500–5008 m. Figure 12 shows the percentage, runoff contribution and runoff coefficient of water balance components on the elevation band scale. The largest area is the elevation band at 3500–4000 m, which accounts for

40.1% of the basin area and contributes 42.2% of the runoff. The runoff coefficient is 0.38, which is close to the runoff coefficient of the entire basin. The elevation band at 4000–4500 m accounts for 25.5% of the basin area and contributes 29.3% of the runoff. This area is featured as cold and wet; thus, the evapotranspiration percentage and soil water content are low, and the runoff coefficient is high. The elevation band at 3500–4500 m accounts for 65.6% of the basin area and contributes 71.5% of the total runoff. Thus, the basin runoff is derived mainly from the high-altitude regions. The elevation band at 2800–3500 m is characterised as warm and dry; thus, precipitation is consumed mainly by evapotranspiration and stored in soil, and the runoff coefficient is low. The elevation band at 4500–5008 m contains a large area of snow and glacier, which exhibits the highest runoff coefficient (0.44) because of snow melting. The elevation band at 1667–2800 m is desert and steppe, and all of the water balance components are low. In summary, climate variability with elevation significantly affects the distribution of water balance components.

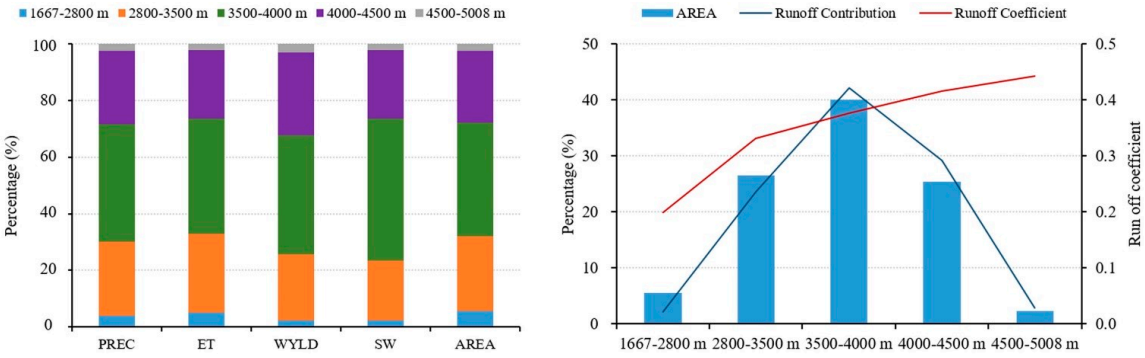

Figure 12. Spatial variability of water balance components at the elevation band scale and runoff coefficient.

4.5.3. Spatial Variability of Water Balance Components at the Sub-Basin Scale

Changes in precipitation are the dominant factor that induces changes in water balance components [38]. Figure 13 shows the spatial variability of the mean annual value of water balance components on the sub-basin scale. The precipitation over the basin ranges from 231 to 670 mm and decreases from the southeast to the northwest. The precipitation of the east tributary is higher than that of the west tributary, and that of the mainstream is the lowest. Evapotranspiration ranges from 220 mm to 560 mm, and the mean value of the entire basin is 306 mm. The water yield ranges from 13 mm to 376 mm and is less than 60 mm in the basin outlet covered by desert. Thus, the underlying surface significantly affects the water yield capacity of the sub-basin. Evapotranspiration exhibits distributions that are similar to those of precipitation. However, the pattern of soil water content varies. The soil water distribution of the east tributary is similar to that of the west tributary because of elevation and landscape, and that of the mainstream is low. The soil water content ranges from 5 mm to 150 mm, and the average value of the entire basin is 52 mm.

The change trend of water balance components can significantly explain the response of hydrological process to climate change. Figure 14 shows the long-term mean annual change trends of water balance components on the sub-basin scale from 2003 to 2014. The precipitation change rate in the entire basin is 0.18 mm·year^{-1}, which indicates a slightly increasing trend. The precipitation increase rate decreases from the southwest to the northwest and varies from −7.4 mm·year^{-1} to 3.55 mm·year^{-1}. The large precipitation increase rate is concentrated in the western basin, and only four sub-basins present a decreasing trend. The increasing evapotranspiration rate decreases from the southeast to the northwest, ranging from −2.51 mm·year^{-1} to 3.6 mm·year^{-1}, with an average value of 0.78 mm·year^{-1}. The water yield decreases in the entire basin (−1.29 mm·year^{-1}), ranging from −11.75 mm·year^{-1} to 2.93 mm·year^{-1}. The spatial distribution of the water yield change rate is consistent with that of precipitation; the increasing trend in the western basin is more obvious than

that in the other regions. The soil water content decreases in the entire basin (-1.18 mm·year^{-1}), ranging from -3.35 mm·year^{-1} to 0.46 mm·year^{-1} at the sub-basin scale.

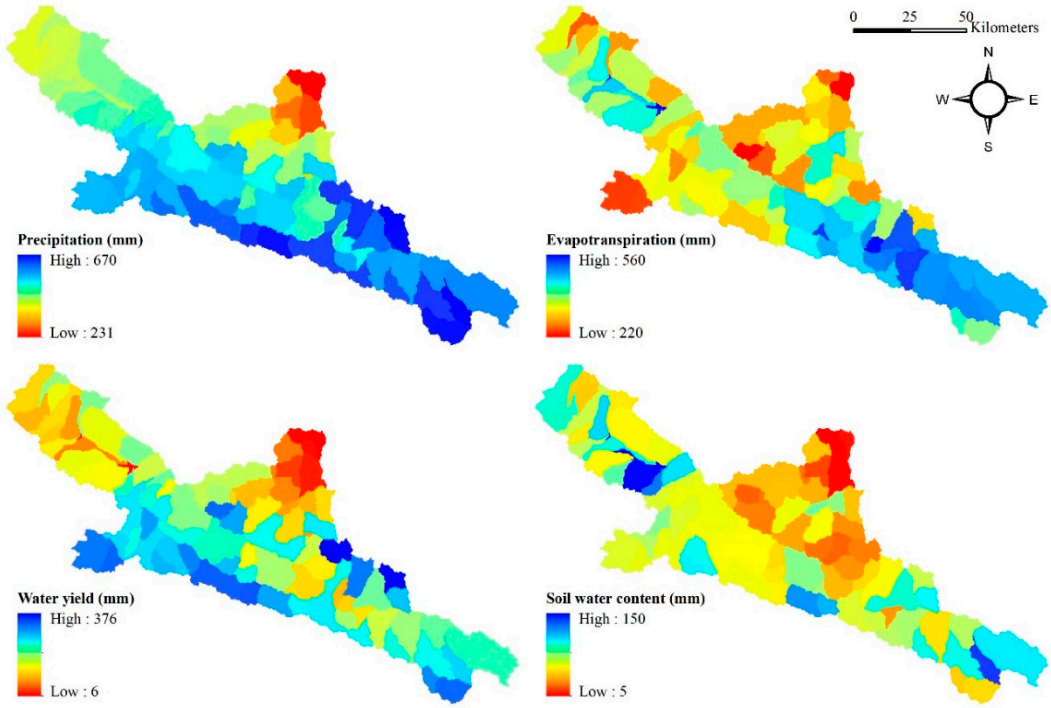

Figure 13. Annual average value of the water balance components at the sub-basin scale from 2003 to 2014.

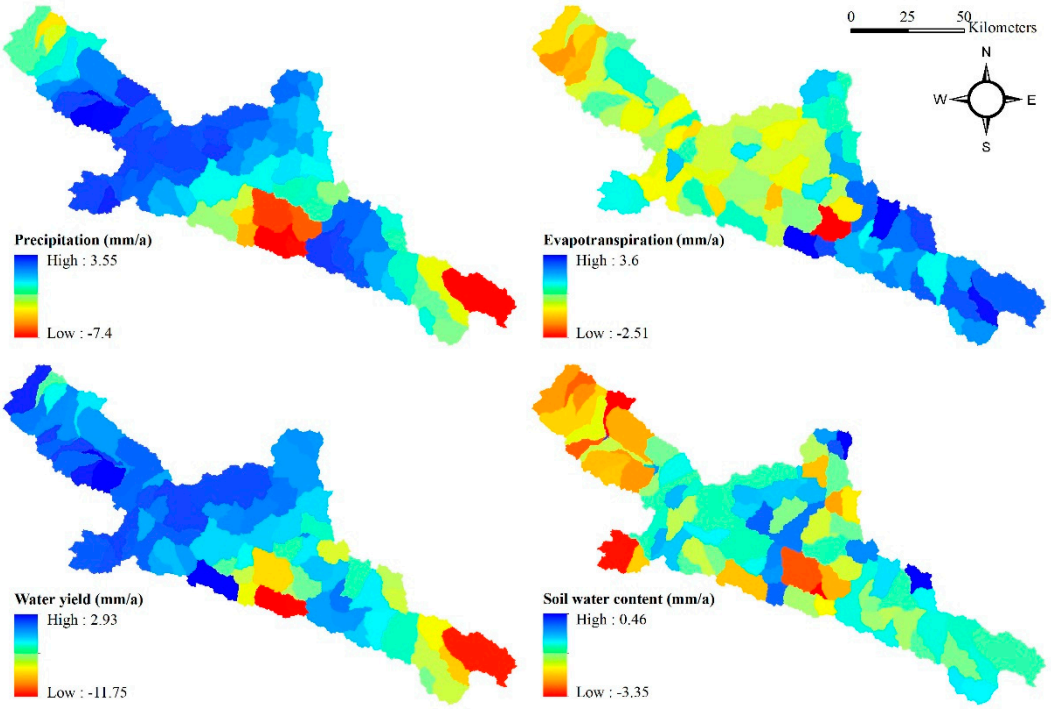

Figure 14. Change trend of the water balance components at the sub-basin scale from 2003 to 2014.

5. Discussion

This study aimed to optimise the input parameters for hydrological simulation using high-resolution gridded precipitation and provide reference for water resource assessment and management in data-scarce regions. The hydrological simulation presents some uncertainties due to uncertainties in input data, model structure, model parameter, and validation data.

Precipitation is an important input for accurate hydrological simulation, and its numerical accuracy and detailed spatial distribution are necessary. The evaluation of gridded precipitation in time series accuracy is used only for two experimental stations and with a short time series (2011–2014). The evaluation of description capability is concentrated on the overall change trend. This data presents high spatial heterogeneity when compared with RIEMS RCM simulation and China National gridded product with a 3 km and 0.25° resolutions, respectively [15]. The description capability of the gridded data is highly reliable. However, these evaluations are insufficient in demonstrating the precision of gridded precipitation because of lack of validation data. Scale transformation is proposed by building virtual precipitation stations and calculating precipitation lapse rate at sub-basin scale, thereby upscaling the gridded data from the grid to sub-basin scale. To some extent, these methods can be used to optimise the precipitation input parameters for the SWAT model effectively and maximise the horizontal and vertical distribution precisions of the high-resolution gridded precipitation. However, the 1113 grids were converted into 97 virtual stations at the sub-basin scale to simplify the spatial distribution of precipitation. Thus, the setting of sub-basin drainage threshold area is significant to scale transformation. The optimal sub-basin drainage threshold area of the sub-basin division based on basin climate and terrain, the division into the sub-basin with a larger number and the building of virtual station with high density are necessary. Previous studies showed that precipitation and elevation can be best described by log-linear or exponential functions [66]. In the present study, linear regression functions were selected because their precipitation lapse rate was considered the mean annual value on the sub-basin scale in the SWAT model. Although this method simplifies the vertical variability of precipitation with elevation, a linear regression function is suitable for calculating the precipitation lapse rate for the SWAT model. For model climate forcing, only precipitation inputs use high-resolution gridded data; the temperature, wind speed, solar ration and relative humidity still use gauged data, which are scarce and unevenly distributed. The high-resolution gridded data of other climate elements should be applied in the SWAT model.

The upper HRB is a typical high cold mountainous region. The process of glacier and permafrost are not considered by the SWAT model. This situation will increase the uncertainty of hydrological simulation. Considering that the glacier area and runoff contribution are low and the glacier area slightly changed in recent years [67], the uncertainty of ignoring the glacier melting runoff have controlled within a reasonable range. In the gentle-elevation catchment, climate uncertainty is relatively low and probably few gauged stations can give reasonable model performance [68]. Precipitation in the upper HRB exhibits a large spatiotemporal variability because of convection in mountainous terrain [50]. Given the complicated mountainous terrain, the high-resolution gridded precipitation is selected for hydrological simulation and analysis; the gridded precipitation was upscaled from the grid to the sub-basin scale. Especially in high mountain regions, this scale transformation method can improve the representation of sub-basin precipitation input data and reducing uncertainty.

After the analysis of parameter sensitivity by SWAT-CUP, the 10 most sensitive parameters were achieved. Furthermore, the parameters with high sensitivity were adjusted to achieve optimal simulation results. The range of parameter calibration was controlled within in $\pm$20%. The daily precipitation event has great uncertainty and randomness. This study concentrated on monthly runoff simulation and annual scale analysis to reduce the uncertainty caused by daily precipitation. The SWAT model achieves excellent monthly runoff simulation on the large-scale and long-term series, which is sufficient to support the study on the water balance component characteristics on the mean annual scale. This result can provide a credible reference for basin water resource assessment and management. Moreover, most hydrological models are simulated monthly runoff in this study area. The current

research can be compared with the previous study. However, the monthly simulation barely reflects the superiority of the gridded precipitation in time series and spatial distribution. Thus, the water balance component characteristics on the daily and small catchment scale should be further investigated.

The SWAT model is widely used in the upper HRB to study hydrological processes, in which NS are usually higher than 0.85 at the monthly scale [7,24–26]. Compared with previous studies that used gauged precipitation, the monthly simulation accuracy derived in the present study has yet to be improved. However, the daily simulation is improved significantly. The dynamic change process of daily runoff response to precipitation events is more obvious. Considering the daily precipitation with a high uncertainty, the daily runoff simulation was assessed in typical normal and high flow year and exhibit high representativeness. Daily simulation is slightly better than monthly simulation based on the model results. Yin et al. [29] and Zou et al. [21] directly inputted gauged precipitation and grid precipitation, respectively, into the SWAT model in the upper HRB. This study used high-resolution gridded precipitation and conducted a scale transformation, which are significantly superior to a few gauged stations and directly input grid data. The precision of model simulation is significantly improved when compared with using grid precipitation as driving data (NS: 0.73). After input precipitation parameters with a high spatial heterogeneity and spatial representation, the spatial distribution of water balance components is more detailed and reasonable and its spatial continuity is better compared with the hydrological simulation based on gauged data and directly input grid data. The model calibration not only relies on hydrographs but also refers to basin features, such as base flow coefficient, evapotranspiration and snow melting runoff. Although the statistical evaluation criteria of simulation are not perfect, the hydrological process and distribution of water balance components are reasonable.

The 15-year simulation present a certain limitation in analysing the change trend of water balance components. In this region, the meteorology and hydrology studies are plentiful and mature in the historical period. On the basis of previous studies [27,34,35], water balance components were analysed on the period of recent years; such study is uncommon. The underlying surface data used by the SWAT model are released in recent years; thus, these data are credible for meteorology and hydrology changing trend analysis in recent years. The precipitation lapse rate, water yield, soil water content and evapotranspiration for data validation lack gauged data that match with the resolution of simulation; thus, the superiority of this study is uncertain. These factors influence the accuracy of the model simulation.

In summary, the uncertainty of scale transformation, model parameter and validation data increase the uncertainty of hydrological simulation. Future studies should focus on these limitations in investigating the SWAT model driven by high-resolution gridded data and in reducing the uncertainty of hydrological simulation.

6. Conclusions

This study considered the upper HRB as a case study, and daily gridded precipitation data with 3 km resolution were selected as forcing data for the SWAT model. Gridded precipitation was subjected to quality assessment and exhibited high time series accuracy and spatial description capability. The scale transformation of gridded precipitation was proposed by building virtual precipitation and calculating precipitation lapse rate on the sub-basin scale. The precision of gridded precipitation in spatial distributions is maximised, and the input precipitation parameters of the SWAT model are optimised. The SWAT model exhibits a good monthly runoff simulation compared with the observed data from 2000 to 2014. The statistical analyses show that the R^2 is higher than 0.71, NS is higher than 0.76, and PBIAS is controlled within $\pm$15%. The base flow coefficient, snow melt runoff, and potential evapotranspiration simulated by the model are consistent with those of previous studies.

The spatial variability of water balance components was analysed on sub-basin, elevation band and landscape scales. The landscape of meadow and sparse vegetation and the band of 3500–4500 m are major water yield region. At the sub-basin scale, the spatial distributions of the water yield

and evapotranspiration are consistent with that of precipitation and decrease from the southeastern to the northwestern areas; the spatial distribution of soil water content is similar to that of the western and eastern areas because of the landscape and elevation band effect; the precipitation and evapotranspiration in the entire basin present a slightly increasing trend, whereas the water yield and soil water content present a slightly decreasing trend. The spatial distribution, change trend, and internal relationship of water balance components across different scales can further strengthen the understanding of the hydrological processes and provide references for the assessment and management of water resources in data-scarce regions.

Acknowledgments: This work was supported by the National Natural Science Foundation of China (grant Nos. 41571031, 91225302, 41601038, and 41601036). The authors are grateful to the Cold and Arid Regions Science Data Centre at Lanzhou (http://westdc.westgis.ac.cn) for data support. The authors thank the editor and three anonymous referees for constructive comments that have significantly improved this work.

Author Contributions: Songbing Zou designed this study. Modeling and analysis was performed by Hongwei Ruan and Songbing Zou; the paper was written by Hongwei Ruan; critical data were provided by Dawen Yang and Yuhan Wang; and Zhenliang Yin, Zhixiang Lu, Fang Li, and Baorong Xu made editing corrections and improvements to the manuscript.

Conflicts of Interest: The authors declare no conflict of interest.

References

1. Deng, X.Z.; Shi, Q.L.; Zhang, Q.; Shi, C.C.; Yin, F. Impacts of land use and land cover changes on surface energy and water balance in the Heihe River Basin of China, 2000–2010. *Phys. Chem. Earth Parts A/B/C* **2015**, *79–82*, 2–10. [CrossRef]
2. Yang, D.W.; Gao, B.; Jiao, Y.; Lei, H.M.; Zhang, Y.L.; Yang, H.B.; Cong, Z.T. A distributed scheme developed for eco–hydrological modeling in the upper Heihe River. *Sci. China Earth Sci.* **2015**, *58*, 36–45. [CrossRef]
3. Deng, X.Z.; Singh, R.B.; Liu, J.G.; Güneralp, B. Water use efficiency and integrated water resource management for river basin. *Phys. Chem. Earth* **2015**, *89*, 1–2. [CrossRef]
4. Gao, B.; Qin, Y.; Wang, Y.H.; Yang, D.W.; Zheng, Y.R. Modeling ecohydrological processes and spatial patterns in the upper Heihe Basin in China. *Forests* **2016**, *7*, 10. [CrossRef]
5. Morrissey, M.L.; Shafer, M.A.; Postawko, S.E.; Gibson, B. The Pacific rain gauge rainfall database. *Water Resour. Res.* **1995**, *31*, 2111–2113. [CrossRef]
6. Yu, M.Y.; Chen, X.; Li, L.H.; Bao, A.M.; Paix, M.J. Streamflow simulation by SWAT using different precipitation sources in large arid basins with scarce raingauges. *Water Resour. Manag.* **2011**, *25*, 2669–2681. [CrossRef]
7. Lu, Z.X.; Zou, S.B.; Xiao, H.L.; Zheng, C.M.; Yin, Z.L.; Wang, W.H. Comprehensive hydrologic calibration of SWAT and water balance analysis in mountainous watersheds in northwest China. *Phys. Chem. Earth* **2015**, *79*, 76–85. [CrossRef]
8. Becker, A.; Finger, P.; Meyer-Christoffer, A.; Rudolf, B.; Schamm, K.; Schneider, U.; Ziese, M. A description of the global land–surface precipitation data products of the Global Precipitation Climatology Centre with sample applications including centennial (trend) analysis from 1901–present. *Earth Syst. Sci. Data* **2013**, *5*, 71–99. [CrossRef]
9. Li, T.; Zheng, X.G.; Dai, Y.J.; Yang, C.; Chen, Z.Q.; Zhang, S.P.; Wu, G.C.; Wang, Z.L.; Huang, C.C.; Shen, Y.; et al. Mapping near–surface air temperature, pressure, relative humidity and wind speed over mainland China with high spatiotemporal resolution. *Adv. Atmos. Sci.* **2014**, *31*, 1127–1135. [CrossRef]
10. Huang, C.C.; Zheng, X.G.; Tait, A.; Dai, Y.J.; Yang, C.; Chen, Z.Q.; Li, T.; Wang, Z.L. On using smoothing spline and residual correction to fuse rain gauge observations and remote sensing data. *J. Hydrol.* **2014**, *508*, 410–417. [CrossRef]
11. Yang, Y.; Wang, G.Q.; Wang, L.J.; Yu, J.S.; Xu, Z.X. Evaluation of gridded precipitation data for driving SWAT model in area upstream of Three Gorges Reservoir. *PLoS ONE* **2014**, *9*, e112725. [CrossRef] [PubMed]
12. Fuka, D.R.; Walter, M.T.; MacAlister, C.; Degaetano, A.T.; Steenhuis, T.S.; Easton, Z.M. Using the Climate Forecast System Reanalysis as weather input data for watershed models. *Hydrol. Process.* **2013**, *28*, 5613–5623. [CrossRef]

13. Shen, Y.; Xiong, A.Y. Validation and comparison of a new gauge–based precipitation analysis over mainland China. *Int. J. Climatol.* **2015**, *36*, 252–265. [CrossRef]
14. Xiong, Z.; Yan, X.D. Building a high–resolution regional climate model for the Heihe River Basin and simulating precipitation over this region. *Chin. Sci. Bull.* **2013**, *58*, 4670–4678. [CrossRef]
15. Wang, Y.H.; Yang, H.B.; Yang, D.W.; Qin, Y.; Gao, B.; Cong, Z.T. Spatial interpolation of daily precipitation in a high mountainous watershed based on gauge observations and a regional climate model simulation. *J. Hydrometeorol.* **2017**, *18*, 845–862. [CrossRef]
16. Qin, Y.; Lei, H.M.; Yang, D.W.; Gao, B.; Wang, Y.H.; Cong, Z.T.; Fan, W.J. Long–term change in the depth of seasonally frozen ground and its ecohydrological impacts in the Qilian Mountains, northeastern Tibetan Plateau. *J. Hydrol.* **2016**, *542*, 204–221. [CrossRef]
17. Arnold, J.G.; Moriasi, D.N.; Gassman, P.W.; Abbaspour, K.C.; White, M.J.; Srinivasan, R.; Santhi, C.; Harmel, R.D.; Van Griensven, A.; Van Liew, M.W.; et al. SWAT: Model use, calibration, and validation. *Trans. ASABE* **2015**, *55*, 1491–1508. [CrossRef]
18. Tobin, K.J.; Bennett, M.E. Using SWAT to model streamflow in two river basins with ground and satellite precipitation data. *J. Am. Water Resour. Assoc.* **2009**, *45*, 253–271. [CrossRef]
19. Evans, J.P. Improving the characteristics of stream flow modeled by regional climate models. *J. Hydrol.* **2003**, *284*, 211–227. [CrossRef]
20. Lakhtakia, M.N.; Yarnal, B.; Johnson, D.L.; White, R.A.; Miller, D.A.; Yu, Z. A simulation of river-basin response to mesoscale meteorological forcing: The Subsequenhanna River Basin Experiment (SRBEX). *JAWRA* **1998**, *43*, 921–937. [CrossRef]
21. Zou, S.B.; Ruan, H.W.; Lu, Z.X.; Yang, D.W.; Xiong, Z.; Yin, Z.L. Runoff simulation in the upper Reaches of Heihe River Basin Based on the RIEMS–SWAT model. *Water* **2016**, *8*, 455. [CrossRef]
22. Sood, A.; Muthuwatta, L.; McCartney, M. A SWAT evaluation of the effect of climate change on the hydrology of the Volta River basin. *Water Int.* **2013**, *38*, 297–311. [CrossRef]
23. Masih, I.; Maskey, S.; Uhlenbrook, S.; Smakhtin, V. Assessing the impact of areal precipitation input on streamflow simulations using the SWAT model. *J. Am. Water Resour. Assoc.* **2011**, *47*, 179–195. [CrossRef]
24. Li, Z.L.; Xu, Z.X.; Shao, Q.X.; Yang, J. Parameter estimation and uncertainty analysis of SWAT model in upper reaches of the Heihe river basin. *Hydrol. Process.* **2009**, *23*, 2744–2753. [CrossRef]
25. Li, Z.L.; Shao, Q.X.; Xu, Z.X.; Cai, X.T. Analysis of parameter uncertainty in semi–distributed hydrological models using bootstrap method: A case study of SWAT model applied to Yingluoxia watershed in northwest China. *J. Hydrol.* **2010**, *385*, 76–83. [CrossRef]
26. Li, Z.L.; Xu, Z.X.; Li, Z.J. Performance of WASMOD and SWAT on hydrological simulation in Yingluoxia watershed in northwest of China. *Hydrol. Process.* **2011**, *25*, 2001–2008. [CrossRef]
27. Zang, C.F.; Liu, J.G. Trend analysis for the flows of green and blue water in the Heihe River basin, northwestern China. *J. Hydrol.* **2013**, *502*, 27–36. [CrossRef]
28. Yin, Z.L.; Xiao, H.L.; Zou, S.B.; Zhu, R.; Lan, Y.C.; Shen, Y.P. Simulation of hydrological process of mountainous watersheds in inland river basin: Taking the Heihe Mainstream River as an example. *J. Arid Land* **2014**, *6*, 16–26. [CrossRef]
29. Yin, Z.L.; Feng, Q.; Zou, S.B.; Yang, L.S. Assessing variation in water balance components in mountainous inland river basin experiencing climate change. *Water* **2016**, *8*, 472. [CrossRef]
30. Thompson, S.E.; Harman, C.J.; Troch, P.A.; Brooks, P.D.; Sivapalan, M. Spatial scale dependence of ecohydrologically mediated water balance partitioning: A systhesis framework for catchment Ecohydrology. *Water Resour. Res.* **2011**, *47*, 143–158. [CrossRef]
31. Gregory, J.M.; David, M.W. Temporal and spatial variability of the global water balance. *Clim. Chang.* **2013**, *120*, 375–387.
32. Herrmann, F.; Keller, L.; Kunkel, R.; Vereechen, H.; Wendland, F. Determination of spatially differentiated water balance components including groundwater recharge on the Federal State level—A case study using them GROWA model in North Rhine–Westphalia (Germany). *J. Hydrol. Reg. Stud.* **2015**, *4*, 294–312. [CrossRef]
33. Jian, S.Q.; Zhao, C.Y.; Fang, S.M.; Yu, K. Effects of different vegetation restoration on soil water storage and water balance in the Chinese Loess Plateau. *Agric. For. Meteorol.* **2015**, *206*, 85–96. [CrossRef]
34. Liu, Y.Q.; Xu, Z.M.; Nan, Z.T. Study on ecological compensation in upper stream of Heihe river basin based on SWAT model and minimum–data approach. *Trans. Chin. Soc. Agric. Eng.* **2012**, *28*, 124–130.

35. Lu, Z.X.; Zou, S.B.; Xiao, H.L.; Yin, Z.L.; Ruan, H.W.; Gao, H.S. How to determine drainage area threshold in alpine regions of upper reaches of Heihe River. *J. Glaciol. Geicryol.* **2015**, *37*, 493–499.
36. Wu, F.; Zhan, J.Y.; Wang, Z.; Zhang, Q. Streamflow variation due to glacier melting and climate change in upstream Heihe River Basin, Northwest China. *Phys. Chem. Earth Parts A/B/C* **2015**, *79*, 11–19. [CrossRef]
37. Kang, E.S.; Cheng, G.D.; Lan, Y.C.; Jin, H.J. A model for simulating the response of runoff from the mountainous watersheds of inland river basins in the arid area of northwest China to climatic changes. *Sci. China Ser. D Earth Sci.* **1999**, *42*, 53–63. [CrossRef]
38. Zhang, A.J.; Liu, W.B.; Yin, Z.L.; Fu, G.B.; Zheng, C.M. How will climate change affect the water availability in the Heihe River Basin, northwest China? *J. Hydrometeorol.* **2016**, *17*, 1517–1542. [CrossRef]
39. Jarvis, A.; Reuter, H.I.; Nelson, A. Hole-Filled SRTM for the Globe Version 4; CGIAR–CSI SRTM 90 m Database. Available online: http://srtm.csi.cgiar.org (accessed on 5 July 2012).
40. Neitsch, S.L.; Arnold, J.G.; Kiniry, J.R.; Williams, J.R. *Soil and Water Assessment Tool Theoretical Documentation Version 2009*; USDA–ARS Grassland, Soil and Water Research Laboratory: Temple, TX, USA, 2011.
41. Neitsch, S.L.; Arnold, J.G.; Kiniry, J.R.; Williams, J.R. *Soil and Water Assessment Tool Theoretical Documentation: Version 2005*; USDA–ARS Grassland, Soil and Water Research Laboratory: Temple, TX, USA, 2005.
42. Gandin, L.S. *Objective Analysis of Meteorological Fields*; Israel Program for Scientific Translations: Jerusalem, Israel, 1965; Volume 242.
43. Paxian, A.; Hertig, E.; Seubert, G.; Vogt, G.; Jacobeit, J.; Paeth, H. Present-day and future mediterranean precipitation extremes assessed by different statistical approaches. *Clim. Dyn.* **2015**, *44*, 845–860. [CrossRef]
44. Price, K.; Purucker, S.T.; Kraemer, S.R.; Babendreier, J.E.; Knightes, C.D. Comparison of radar and gauge precipitation data in watershed models across varying spatial and temporal scales. *Hydrol. Process.* **2013**, *28*, 3505–3520. [CrossRef]
45. Tuo, Y.; Duan, Z.; Disse, M.; Chiogna, G. Evaluation of precipitation input for SWAT modeling in alpine catchment: A case study in the Adige river basin (Italy). *Sci. Total Environ.* **2016**, *573*, 66–82. [CrossRef] [PubMed]
46. Zhang, A.J.; Zheng, C.M.; Wang, S.; Yao, Y.Y. Analysis of streamflow variations in the Heihe River Basin, northwest China: Trends, abrupt changes, driving factors and ecological influences. *J. Hydrol. Reg. Stud.* **2015**, *3*, 106–124. [CrossRef]
47. Liu, J.F.; Chen, R.S.; Qin, W.W.; Yang, Y. Study on the vertical distribution of precipitation in mountainous regions using TRMM data. *Adv. Water Sci.* **2011**, *22*, 447–454.
48. Chen, R.S.; Song, Y.X.; Kang, E.S.; Han, C.T.; Liu, J.F.; Yang, Y.; Qing, W.W.; Liu, Z.W. A Cryosphere–Hydrology Observation System in a small alpine watershed in the Qilian Mountains of China and is meteorological gradient. *Arct. Antarct. Alp. Res.* **2014**, *46*, 505–523. [CrossRef]
49. Chang, X.X.; Zhao, A.F.; Wang, J.Y.; Chang, Z.Q.; Jin, B.W. Precipitation Characteristic and Interception of Forest in Qilian Mountain. *Plateau Meteorol.* **2002**, *21*, 274–280.
50. Ding, Y.J.; Ye, B.S.; Zhou, W.J. Temporal and spatial precipitation distribution in the Heihe Catchment, Northwest China, during the past 40 a. *J. Glaciol. Geocryol.* **1999**, *21*, 42–48.
51. Legates, D.R.; McCabe, J. Evaluating the use of "Goodness-of-Fit" measures in hydrologic and hydroclimatic model validation. *Water Resour. Res.* **1999**, *35*, 233–241. [CrossRef]
52. Gupta, H.V.; Sorooshian, S.; Yapo, P.O. Status of automatic calibration for hydrologic models: Comparison with multilevel expert calibration. *J. Hydrol. Eng.* **1999**, *4*, 135–143. [CrossRef]
53. Singh, J.; Knapp, H.V.; Arnold, J.G.; Demissie, M. Hydrologic modeling of the Iroquois River watershed using HSPF and SWAT. *J. Am. Water Resour. Assoc.* **2005**, *41*, 343–360. [CrossRef]
54. Wang, N.L.; He, J.Q.; Jiang, X.; Song, G.J.; Pu, J.C.; Wu, X.B.; Chen, L. Study on the zone of maximum precipitation in the north slopes of the central Qilian mountains. *J. Glaciol. Geocryol.* **2009**, *31*, 396–403.
55. Li, X.; Cheng, G.D.; Liu, S.M.; Xiao, Q.; Ma, M.G.; Jin, R.; Che, T.; Liu, Q.H.; Wang, W.Z.; Qi, Y.; et al. Heihe watershed allied telemetry experimental research (HiWATER): Scientific objectives and experimental design. *Bull. Am. Meteorol. Soc.* **2013**, *94*, 1145–1160. [CrossRef]
56. Wang, J.; Li, S. Effect of climatic change on snowmelt runoffs in mountainous regions of inland rivers in Northwestern China. *Sci. China Ser. D Earth Sci.* **2016**, *49*, 881–888. [CrossRef]
57. Zhao, D.Z.; Zhang, W.C. Rainfall–runoff simulation using the VIC–3L model over the Heihe River mountainous basin, China. In Proceedings of the 2005 IEEE International Geoscience and Remote Sensing Symposium, Seoul, Korea, 29 July 2005; Volume 6, pp. 4391–4394.

58. Jia, Y.; Ding, X.; Qin, C.; Wang, H. Distributed modeling of landsurface water and energy budgets in the inland Heihe river basin of China. *Hydrol. Earth Syst. Sci.* **2009**, *13*, 1849–1866. [CrossRef]
59. Li, Z.; Liu, W.Z.; Zhang, X.C.; Zheng, F.L. Impacts of land use change and climate variability on hydrology in an agricultural catchment on the Loess Plateau of China. *J. Hydrol.* **2009**, *377*, 35–42. [CrossRef]
60. Xu, B.R.; Lu, Z.X.; Liu, S.Y.; Li, J.; Xie, J.L.; Long, A.H.; Yin, Z.L.; Zou, S.B. Glacier changes and their impacts on the discharge in the past half–century in Tekes watershed, Central Asia. *Phys. Chem. Earth* **2015**, *89*, 96–103. [CrossRef]
61. Nash, J.E.; Sutcliffe, J.V. River flow forecasting through conceptual models: Part 1. A discussion of principles. *J. Hydrol.* **1970**, *10*, 282–290. [CrossRef]
62. Zhang, H.; Zhang, B.; Zhao, C.Y. Annual base flow change and its causes in the upper reaches of Heihe River. *Geogr. Res.* **2011**, *30*, 1411–1430.
63. Wu, B.F.; Yan, N.N.; Xiong, J.; Bastiaanssen, W.; Zhu, W.; Stein, A. Validation of ETWatch using field measurements at diverse landscapes: A case study in Hai Basin of China. *J. Hydrol.* **2012**, *436*, 67–80. [CrossRef]
64. Moriasi, D.N.; Arnold, J.G.; Van Liew, M.W.; Bingner, R.L.; Harmel, R.D.; Veith, T.L. Model evaluation guidelines for systematic quantification of accuracy in watershed simulations. *Trans. ASABE* **2007**, *50*, 885–900. [CrossRef]
65. He, Z.B.; Zhao, W.Z.; Liu, H.; Tang, Z.X. Effect of forest on annual water yield in the mountains of an arid inland river basin: A case study in the Pailugou catchment on northwestern China's Qilian Mountains. *Hydrol. Process.* **2012**, *26*, 613–621. [CrossRef]
66. Daly, C.; Neilson, P.R.; Phillips, D.L. A statistical–topographic model for mapping climatological precipitation over mountainous terrain. *J. Appl. Meteorol.* **1994**, *33*, 140–158. [CrossRef]
67. Wei, J.F.; Liu, S.Y.; Guo, W.Q.; Yao, X.J.; Xu, J.L.; Bao, W.J.; Jiang, Z.L. Surface–area changes of glaciers in the Tibetan Plateau interior area since the 1970s using recent Landsat images and historical maps. *Annu. Glaciol.* **2014**, *55*, 213–222.
68. Jamilatou, C.B.; Seifeddine, J.; Sihem, B.; Pibgnina, B.; Abel, A.; Michael, R. Multi-Site Validation of the SWAT Model on the Bani Catchment: Model Performance and Predictive Uncertainty. *Water* **2016**, *8*, 178. [CrossRef]